

Light Curves of Microlensed Type Ia Supernovae

Hamed Bagherpour ¹, Ronald Kantowski ², David Branch ³

*University of Oklahoma, Department of Physics and Astronomy,
Norman, OK 73019, USA*

Dean Richardson ⁴

*Denison University, Department of Physics and Astronomy,
Granville, OH 43023, USA*

ABSTRACT

A detailed description of the apparent light curves of microlensed SNe Ia as extended and expanding sources is presented. We show that microlensing amplification can have significant effects on supernova observation. A model light curve is used to compare lensed and unlensed cases and we find that significant changes in shape can occur because of microlensing. We briefly discuss the probability of observing such effects as well. Throughout the paper we consider source and deflector redshifts at 1.0 and 0.05 respectively, and limit our work to spherically symmetric deflectors.

Subject headings: gravitational lensing — supernovae: general

1. Introduction

Out of a number of distance indicators, supernovae have emerged as the most promising standard candles. Due to their significant intrinsic brightness and relative ubiquity they can be observed in the local and distant universe. Several teams including the High-z Supernova Search (Schmidt et al. 1998) and the Supernova Cosmology Project (Perlmutter et al. 1999)

¹hamed@nhn.ou.edu

²kantowski@nhn.ou.edu

³branch@nhn.ou.edu

⁴richardson@denison.edu

have been searching for supernovae at higher redshifts since the early 1990’s. Light emitted from these ‘standard candles’ is subject to lensing by intervening objects while traversing the large distances involved (Kantowski, Vaughan, & Branch 1995); the further the light source, the higher its chance of being significantly lensed. In fact, for cosmologically distant sources, the probability is high that a distant point source will be ‘imaged’ (Press & Gunn 1973; Bourassa & Kantowski 1976; Wyithe & Turner 2002), particularly by stellar-size objects (microlensing). While the systematic errors introduced by K-correction, selection effects, and possible evolution can be removed, lensing might ultimately limit the accuracy of luminosity distance measurements (Perlmutter & Schmidt 2003). Only a large sample of SNe at each redshift can be used to characterize the lensing distribution and to correct for the effect of lensing.

Properties of microlensed supernovae have been studied previously. Schneider & Wagoner (1987) presented the time-dependent amplification of supernovae caused by the expansion of the photosphere, and showed that the related polarization of a supernova is not likely to exceed 1%. For cosmologically distant supernovae a 1% effect is practically impossible to detect. Linder, Schneider, & Wagoner (1988) studied amplification of supernovae and developed approximate formulae for the amplification probability distribution. Rauch (1991) studied microlensing of SNe Ia by compact objects and calculated the resulting amplification probability distributions using Monte Carlo simulations. Kolatt & Bartelmann (1998) calculated the light curves of type Ia supernovae microlensed by intracluster MACHO’s assuming the point-deflector (with shear) model of Chang & Refsdal (1984).

In this paper, we demonstrate how microlensing by a single stellar-size deflector can affect light curves of cosmologically distant SNe Ia. We use the simple Schwarzschild lens model to calculate amplifications. We ignore the additional amplification caused by the macrolensing introduced by the hosting galaxy, and concentrate on the time dependent effects caused by a single moving stellar-size deflector. We model the SNe Ia by expanding light sources with realistic radial surface intensity profiles.

In the next section, we present a model light curve for type Ia supernovae. § 3 is devoted to a brief review of the gravitational lensing effect, and in § 4 we present the results of our calculations. Throughout, we assume a flat Friedmann-Lemaître-Robertson-Walker cosmological model with $\Omega_m = 0.3$, $\Omega_\Lambda = 0.7$, and $h_{100} = 0.67$ to calculate the distances to the source and deflector.

2. Light Curves of Type Ia Supernovae

In general, spectacular supernovae explosions can be interpreted in terms of two concepts (Arnett 1996): A shock wave running through a stellar envelope, and the radioactive decay of newly synthesized ^{56}Ni to ^{56}Co and then to ^{56}Fe . The nature of the explosion is the expansion away from the region of energy release. The explosion becomes more spherically symmetric with time, trending toward a small-scale Hubble type flow.

In the meantime, various aspects of the event including shock emergence, radiative diffusion, heating, and recombination determine the evolution of the luminosity, i.e., the light curve, which is usually exhibited as the absolute magnitude as a function of time. In the case of SNe Ia, it is the shape of the light curve that can be used to measure cosmological parameters such as Hubble constant; see, for instance, Riess, Press, & Kirshner (1995).

To model the intrinsic Type Ia supernova light curve we used a combination of two existing analytical models; for the peak of the light curve (early time) we used the model of Arnett (1982) while for the tail of the light curve (late time) we used the deposition function described by Jeffery (1999). The basic assumptions made in this model are: a homologous expansion of the photosphere, radiation pressure dominates at early times, the diffusion approximation is valid at early times, the optical opacity is constant for the light curve peak and the gamma-ray opacity is constant for the tail, ^{56}Ni is present in the ejecta and its distribution is peaked toward the center of the ejected mass at small initial radius. The details of this combined model are in Richardson, Branch, & Baron (2005). The model parameters have been fixed for a typical SN Ia: the kinetic energy is 1 foe (10^{51} erg), the total ejected mass is $1.4 M_{\odot}$, and the ^{56}Ni mass has been set to $0.6 M_{\odot}$. These values produce a SN Ia with a peak absolute magnitude of about -19.5.

To test the model we varied the kinetic energy, nickel mass, and the rise time until we achieved the best χ^2 fit to the observed data of a few SNe Ia. The model worked well as can be seen in Figure 1, where the fit of SN1990N is shown with $E_k = 0.60$ foe, $M_{Ni} = 0.62 M_{\odot}$, $t_{rise} = 21$ days, and the reduced $\chi^2 = 0.43$. We use this supernova because it was well observed (the light curve had good coverage) and it is photometrically characteristic of most SNe Ia.

3. Microlensing of Extended Sources

3.1. Basics

The linearized Einstein theory for a static gravitational field gives a bending angle for light rays passing through a weak gravitational field of

$$\boldsymbol{\alpha} = -\frac{2}{c} \int_{-\infty}^{+\infty} \nabla \phi dt, \quad (1)$$

where ϕ is the Newtonian gravitational potential satisfying the boundary conditions $\phi \rightarrow 0$ at infinity, and where the integral is performed along the light path in the absence of the gravitational field. For a point deflector the bending angle is simply

$$\boldsymbol{\alpha} = -\frac{4Gm_d}{c^2 r} \hat{\mathbf{r}}, \quad (2)$$

where \mathbf{r} is the light ray's impact vector and M_d is the deflector's mass. Bourassa, Kantowski, & Norton (1973), and Bourassa & Kantowski (1974, 1976) used the 2-component nature of $\boldsymbol{\alpha}$ to replace it with the complex scattering function $I(z)$, where $z = x + iy$ is the complex equivalent of the 2-d vector $\mathbf{r} = x\hat{i} + y\hat{j}$. Using $I(z)$, the relation between the source position, z , and image position, z_o , when both are projected onto the plane of the deflector (also called the sky plane) is

$$z = z_o - \frac{4GD}{c^2} I^*(z_o). \quad (3)$$

The scaled (effective) distance D is defined as $D = D_{ds}D_d/D_s$, where the deflector-source distance, D_{ds} , the observer-deflector distance, D_d , and the observer-source distance, D_s , are all the same type distances, e.g., apparent size distances.

In the case of a point deflector (on which we focus in this paper), the scattering function takes a very simple form:

$$I(z_o) = \frac{m_d}{z_o}, \quad (4)$$

and the equation (3) reduces to

$$z = z_o - \frac{r_E^2}{z_o^*}, \quad (5)$$

where $r_E \equiv \sqrt{4Gm_d D c^{-2}} = \sqrt{2r_S D}$ is the Einstein ring radius, and r_S is the deflector's Schwarzschild radius. This equation has two separate solutions (images) for any source position $r = |z|$,

$$r_p = |z_p| = \frac{1}{2} \left(\sqrt{r^2 + 4r_E^2} + r \right),$$

and

$$r_s = |z_s| = \frac{1}{2} \left(\sqrt{r^2 + 4r_E^2} - r \right). \quad (6)$$

Both images are in line with source and deflector. The ‘primary’ image, r_p , lies on the same side of the deflector while the ‘secondary’ image, r_s , is on the other side (Fig. 2). In the case of microlensing, the angular separation of the two images ($\theta_p + \theta_s$ in Fig. 2) is of the order of micro arcseconds. Consequently, the two images are seen as a single object (§ 3.2). The Einstein ring occurs when source and deflector are aligned with the observer ($r = |z| = 0$) for which $r_p = r_s = r_E$, and due to the symmetry of the lensing configuration the image is actually a ring. For a point deflector, the primary image is outside the Einstein ring ($r_p \geq r_E$) while the secondary image falls inside ($r_s \leq r_E$) as can be seen in Figure 3.

The effect of gravitational lensing on the apparent brightness of a distant source can be computed in various ways. For extended sources like supernovae it is best to employ the fact that the apparent brightness is proportional to the image’s apparent area, meaning that the brightness of a source is amplified by a factor A :

$$A = \frac{\mathcal{A}_o}{\mathcal{A}}, \quad (7)$$

where \mathcal{A}_o is the area of the image and \mathcal{A} is the area of the source both projected on the deflector plane. For a point mass deflector and a small point-like source the amplification of the primary and secondary images respectively can be written as

$$A_p = \frac{r^2 + 2r_E^2}{2r\sqrt{r^2 + 4r_E^2}} + \frac{1}{2},$$

and

$$A_s = \frac{r^2 + 2r_E^2}{2r\sqrt{r^2 + 4r_E^2}} - \frac{1}{2}. \quad (8)$$

If the images are unresolvable the combined amplification becomes

$$A \equiv A_p + A_s = \frac{r^2 + 2r_E^2}{r\sqrt{r^2 + 4r_E^2}}. \quad (9)$$

If the source is not small, i.e., if r/r_E varies significantly across the source, differential amplification must be taken into account. Measuring this amplification from a single observation is not possible since it is practically impossible to figure out the original source flux. However, if the luminosity of the source varies with time in a predictable way as with SNe or if the source is of constant brightness and the lens is moving with respect to the line of sight to the source [as with observation of bulge stars; see, for instance, Sumi et al. (2004)], the

amplification will change with time in a predictable way and it is possible to determine the amplification. Figure 4 shows amplification curves of a point source lensed by a spherically symmetric deflector with mass $m_d = 1 M_\odot$.

The relative time delay of the two images (which is due to both the geometrical path difference of the two light signals and the difference in the gravitational potential through which the light rays travel (Cooke & Kantowski 1975) turns out to be only a small fraction of a second as expected for microlensing. Such small time delays between the two images can therefore have no effect on microlensed supernova light curve when features change on time scales of days or greater.

3.2. Amplification of an Extended Source

As implied in the last section, to obtain the total flux received from an extended source, an integral of intensity across the source may be required:

$$A = \frac{\int_{image} I d\mathcal{A}_o}{\int_{source} I d\mathcal{A}}. \quad (10)$$

If the surface brightness is constant across the source or if there is no differential amplification, the net amplification is simply given by equation (7), where \mathcal{A}_o can be the primary, secondary, or total image area, giving respectively the primary, secondary, or total amplification. In the case of a circular extended source with a projected radius of a at a distance l from the center of a spherically symmetric deflector (a and l are measured in the deflector plane), the total area of the combined and unresolvable images is

$$\mathcal{A}^{(total)} = \int_{-\frac{\pi}{2}}^{\frac{\pi}{2}} a (a + l \sin \varphi) \sqrt{1 + \frac{4r_E^2}{l^2 + a^2 + 2al \sin \varphi}} d\varphi \quad (11)$$

After a rather long calculation, the total amplification is found to be

$$A[a, l, r_E] = \eta \{ \mu_1 K(k) + \mu_2 E(k) + \mu_3 \Pi(n, k) \}, \quad (12)$$

(Witt & Mao 1994; Mao & Witt 1998) where K , E , and Π are respectively the first, second, and third complete elliptic integral with

$$k = \frac{16alr_E^2}{(l+a)^2((l-a)^2 + 4r_E^2)},$$

$$n = \frac{4al}{(a+l)^2},$$

and constants

$$\begin{aligned}
 \eta &= \frac{1}{2\pi a^2 \sqrt{(l-a)^2 + 4r_E^2}}, \\
 \mu_1 &= (l-a)(a^2 - l^2 - 8r_E^2), \\
 \mu_2 &= (l+a)((l-a)^2 + 4r_E^2), \\
 \mu_3 &= \frac{4(l-a)(a^2 + r_E^2)}{l+a}.
 \end{aligned} \tag{13}$$

Using equations (8) and (9), equation (12) gives amplifications for both the primary and secondary images. Figure 5 is a plot of the amplification curves of an extended source moving with speed 0.5 AU per day ($1 \text{ AU day}^{-1} \simeq 1.73 \times 10^3 \text{ km s}^{-1}$) with respect to a deflector of mass $1 M_\odot$. To illustrate combined effect of relative motion and finite size on amplification, in Figure 5 we have assumed a constant surface brightness across the source (no limb darkening) and a fixed radius of 178 AU, corresponding to that of a supernova with a maximum atmospheric speed of 30,000 kilometer per second at eighteen days after the explosion. In Figure 5, the source approaches the deflector with various impact parameters (closest approach), producing different amplification curves.

In what follows we use a more realistic supernova model to calculate amplification curves. We assume a ring-like structures for the intensity I of a spherically expanding photosphere like that of a SN Ia (Höflich 1990). To model the 2-dimensional brightness profile across the source we assumed that the emissivity of light coming from any volume element in the photosphere of a type Ia supernova is constant. We found

$$I(r) = I_o \sqrt{1 - \left(\frac{r}{r_{ph}}\right)^2}, \tag{14}$$

where I_o is the intensity at the center and r_{ph} is the radius of the photosphere. This profile is in agreement with one of the commonly used family of limb-darkening profiles (Allen 1973; Claret, Díaz-Corovés, & Giménez 1995). The assumption that emissivity per volume in SNe Ia is constant is a reasonable assumption during the nebular phase ($t > 150$ days). To see whether the obtained intensity profile is also applicable to photospheric phase ($t < 150$ days) we compared it to a normalized intensity distribution function (IDF) calculated using W7 model (Nomoto, Thielemann, & Yokoi 1984) for SNe type Ia in U and B bands (courtesy of E. Lentz). The result of this IDF calculation as well as our intensity profile can be seen in Figure 6. The two models show a reasonable match.

We also estimated the characteristic radius of the optical image of a type Ia supernova as a function of time. For the photospheric phase, we assumed homologous expansion ($r=vt$)

and obtained the radius of the photosphere as a function of time since explosion by multiplying the speed at the photosphere, as determined empirically by Branch et al. (2005), by the time. For the nebular phase, we assumed that the radius of the iron–group core expands at a constant velocity of 6000 km s^{-1} . A good fit for the speed is an exponential:

$$v = 9.1 e^{(-t/36.5 \text{ days})} + 6.0, \quad (15)$$

in units of 10^3 km s^{-1} . Figure 7 shows the expansion velocity as well as the radius as a function of time.

3.3. Probability

The relevant quantity in seeing a microlensing event is the optical depth τ . It is defined as the probability that a point source (or equivalently the center of an extended source) falls inside the Einstein ring of some deflector. The brightness of a point source within r_E is amplified by a factor of at least 1.34. For randomly located point deflectors the optical depth depends on the mass density of the deflectors and not on their number density (Press & Gunn 1973).

Typical values of the optical depths for microlensing of nearby luminous sources are remarkably small. For instance, Sumi et al. (2003) calculated an optical depth $\tau = 2.59_{-0.64}^{+0.84} \times 10^{-6}$ toward the Galactic Bulge (GB) in Baade’s window for events with time scales between 0.3 and 200 days. Because of the small value of τ , millions of stars need to be monitored when searching for microlensing in areas such as the GB, the Large Magellanic Cloud, or the Small Magellanic Cloud. The value of τ is much higher for cosmologically distant sources. Assuming that the ordinary stellar populations of galaxies are the dominant causes of microlensing events, Wyithe & Turner (2002) concluded that in a flat universe, at least 1% of high-redshift sources ($z_s \geq 1$) are microlensed by stars at any given time. Zakharov, Popović, & Jovanović (2004) estimated that the optical depth for microlensing caused by deflectors both localized in galaxies and distributed uniformly, might reach 10% for sources at $z_s \sim 2$. If we look at bulge-bulge lensing, Han & Gould (2003) give a model for the bulge from which a value of $\tau = 0.98 \times 10^{-6}$ is computed. They additionally compute an effective column density for deflectors $\Sigma_* = 2086 \text{ M}_\odot \text{ pc}^{-2}$ and a characteristic source-lens separation $\overline{D} = 782 \text{ pc}$ defined by

$$\tau = \frac{4\pi G}{c^2} \Sigma_* \overline{D}. \quad (16)$$

If we simply look at the bulge of a similar galaxy at $z = 0.05$ we expect a similar Σ_* but \overline{D} becomes the distance to the deflector D_d and hence increased by a factor $\approx 2.7 \times 10^5$. This would bring the optical depth up to 27% when looking through such a galaxy. At

this distance the size of the bulge is ~ 1 arcsec and clearly resolvable. The downside is one of alignment. What is the chance of a host galaxy being appropriately aligned with a foreground galaxy? The best place to see this effect seems to be the foregrounds of dense clusters. Because the typical galaxy is expected to contain a SNIa every 10^3 yrs, some $3700(1+z)$ alignments would have to be followed for a year to see one event.

As mentioned above, the amplification of a point source falling inside the Einstein ring r_E is larger than 1.34. The probability of a larger amplification is proportionally smaller. The probability of having an amplification larger than A for a given lensing configuration is

$$p(A) = u_A^2 \tau(z_s), \quad (17)$$

where $u_A \equiv b_A/r_E$ is the normalized impact parameter, resulting in amplification A (Paczynski 1986a,b) and $\tau(z_s)$ is the optical depth for a source at redshift z_s . For a point source, the result is

$$u_A = \sqrt{2 \left(\frac{A}{\sqrt{A^2 - 1}} - 1 \right)}. \quad (18)$$

In the next section we use (17) to reduce the optical depth to probabilities appropriate for higher amplifications.

4. Microlensed Light Curves

In this section we use the model light curve of § 2 and the microlensing theory of § 3 to predict the shape of lensed light curves of type Ia supernovae. We have calculated absolute magnitudes of the lensed SNe type Ia in the V-band. We assume that the source is at redshift $z_s = 1.0$, hence introducing a time dilation factor of $(z+1)^{-1} = 0.5$, and is lensed by a deflector located at redshift $z_d = 0.05$. Figure 8 shows the geometry of our model. To calculate the amplification as a function of time (eq. [12]), we need to know the distance l between the supernova and the deflector, projected on the plane of the deflector,

$$l(t) = \sqrt{l_o^2 + vt \left(vt \mp 2\sqrt{l_o^2 - b^2} \right)}, \quad (19)$$

where the minus sign is used when the supernova source explodes ($t = 0$ and $l = l_o$) before getting to the point of closest approach, b , and the plus sign when it explodes after. We also need the Einstein ring radius r_E which is determined by the mass of the deflector m_d and the distances of the supernova and the deflector from the observer.

We plot light curves for various values of parameters m_d , b , l_o , and v (the relative speed of source and deflector projected on the deflector's plane). Our sample deflector masses are

$10^{-3} M_{\odot}$, $1 M_{\odot}$, and $10 M_{\odot}$. We take the source to move in the deflector plane for 1,000 days (observer time) with two relative projected speeds of the source v , 0.1 AU day^{-1} and 0.5 AU day^{-1} .

Figures 9 through 17 show the amplification curves (upper panels) and the light curves (lower panels) of lensed supernova for nine different sets of input parameters. These interesting cases have been selected from a large number of configurations. The top panel of each figure shows the amplification of the primary and secondary images as well as their sum (total amplification), and the bottom panel includes light curves of the two images and their sum (the apparent light curve) as well as the original (unlensed) light curve of the supernova.

We are plotting amplified absolute magnitudes of the supernova in the V-band, however, due to the redshift of the source, these light curves would be observed in the I-band. With the source located at $z_s = 1$, $M_V > -17$ is too dim to be seen. Nonetheless, we include the complete amplification and light curves to show their trends over a period of 1,000 days after the supernova explosion.

We can easily match the features in the light curve in each figure to the corresponding peak of the amplification curve. Figure 9 shows a huge overall increase in the brightness of the whole light curve. For this case the SN explosion occurs when the SN is near minimum impact $l_0 = b = 0$. The amplification is strongest around the peak so the largest decrease in M_V happens there (almost 5 magnitudes). If the mass of the deflector were increased to $10 M_{\odot}$ the magnitude of the ‘narrowed’ peak would reach $M_V \sim -26$ which is comparable to the magnitude of a bright quasar. Such huge amplifications can cause a bias in observing supernovae, allowing one to observe more distant supernovae, and as a result, to increase the depth (volume) of any supernova survey. Notice that this light curve looks different from those of strongly lensed supernovae in which, the lensed curve merely has an overall magnitude shift upward due to the static magnification introduced by the microlens’ parent galaxy.

In Figures 10 and 11, the lensed light curve hits a plateau before falling back on the expected trend of a type Ia supernova. For some values of the input parameters it is possible to observe a second peak in the light curve, e.g., see Figures 12 through 17. The second peak in each of these figures is bright enough to be observed and could easily be distinguished from the original (first) peak. If the impact parameter in Figure 12 is reduced to $b = 0$ the second peak would actually be larger than the first. Figure 17 is another example of a second peak in the light curve which is bright enough to be seen although it occurs more than 400 days after the supernova explosion. If the position of the initial explosion were increased to $l_0 = 0.1$ the still visible second peak would occur 2 years after the first. For many cases, microlensing has a less dramatic effect on the light curve’s shape; it simply provides an

overall increase in its magnitude, and would be difficult to distinguish from amplification due to the galaxy hosting the microlens.

The interesting cases described above occurred because the supernova exploded within the Einstein ring of a deflector, while the deflector proceeded to move on a time scale comparable to the life of the supernova. Schneider & Wagoner (1987) found, in some instances, similar double peak modifications to the light curve caused by the supernova’s photosphere expanding into a deflector’s critical point.

The standard optical depth τ significantly overestimates the probability that the above interesting cases will occur. Using § 3 we can correct for the overestimate. For these lensing configurations, the normalized impact parameter u_A does not exceed 0.1 ($A \approx 9$) which, using equation (17), gives a maximum probability of $\sim 10^{-4}$ for $z_s \geq 1$ ($\tau = 0.01$), and $\sim 10^{-3}$ for $z_s = 2$ ($\tau = 0.1$) if Zakharov, Popović, & Jovanović (2004) are correct. These numbers are somewhat higher than Linder, Schneider, & Wagoner (1988) were predicting for Type I SN but not for Type II. With a supernova rate of $R_{SNeIa} = 2,000 \text{ yr}^{-1}$ the SN lensing rate at redshift $z = 1$ is $\sim 10^{-4} \Omega \text{ yr}^{-1}$ (Oguri, Suto, & Turner 2003). Rates like this, together with time scales of some cases studied here, imply that such effects may not be observed unless a large number of cosmologically distant (around 10^4 for $z_s \geq 1$) type Ia supernovae are followed for a period of up to 2 years. For the high amplification cases with a second peak, a separate probability estimate can be made (see the Appendix).

5. Conclusion

We have shown that microlensing can significantly affect the light curve of a cosmologically distant type Ia supernova. We restricted our calculation to $z_s = 1$ and $z_d = 0.05$ in the currently accepted $\Omega_m = 0.3$, $\Omega_\Lambda = 0.7$ flat cosmological model. We found that microlensing not only increases the magnitude of the light curve but also can cause a change in its shape. Relative transverse motion of the SN and lens, as well as the expanding photosphere (Schneider & Wagoner 1987) can result in features such as a narrow but high peak, a plateau following the peak, or even the presence of a second peak.

In § 4 we concluded that for microlensing by compact masses distributed through the cosmos, the optical depth is 0.01 ($z_s \sim 1$) but might reach 0.1 ($z_s \sim 2$), meaning that the overall chance of a distant supernova type Ia being microlensed is not negligible. Any multi-band supernova survey aimed at finding supernovae at redshifts around $z = 1$ (and above), could discover and identify *one* microlensed SN Ia event out of roughly *a hundred* events. However, the low impact parameters required to produce the special features depicted in §

4 demand observation of $\sim 10^4$ supernovae at $z_s \geq 1$. And, to see unusual features such as double peaks, the lensed supernova must be followed for an extended period of ~ 2 years. In the Appendix we have made an optical depth type estimate to include double peak events. For microlensing by stars in the bulge of a galaxy at $z_d = 0.05$ we find a max probability of $\sim 1.7 \times 10^{-3}$. This is an ideal deflector distance for observing double peaks due to transverse motion. As expected this number is only slightly smaller than the 27% optical depth estimate made in §3.3 for bulge lensing when corrected for an impact $u = 0.1$. These estimates do not take into account the observational bias in favor of amplified events (§ 4) nor the possibly enhanced probability due to evolution of the rate at which Type-Ia supernovae have occurred. It is interesting to note that according to OGLE III (Udalski 2003) a histogram of u values for Bulge lensing peaks at $u \sim 0.1$ (probably due to amplification biasing).

The authors are pleased to thank an anonymous referee for helpful criticisms of the first version of the manuscript and Zach Blankenship for correcting an oversight in this version. This work was in part supported by NSF grant AST0204771 and NASA grant NNG04GD36G.

A. Appendix

In this appendix we compute the probability that a source, followed for a period T , impacts a point deflector with a reduced impact parameter less than $u \equiv b/R_E$ and simultaneously moves at least a distance b during the period T . Such a time dependent impact will cause a change in the amplification of 10%-50% depending on the actual impact. The idea here is to estimate the chance of seeing a distortion in the light curve of a SN whose life time is $T_{SN} \sim 200$ days.

We start with a number density N_d of mass m deflectors (located at a distance D_d from the observer) moving with relative transverse velocities distributed according to:

$$\frac{dN_d}{dv} = N_d(D_d) \frac{v}{v_{rms}^2} e^{-v^2/2v_{rms}^2}. \quad (\text{A1})$$

The probability of one of these moving deflectors impacting the line of sight to a source at D_s with a reduced impact parameter $\leq u$ and moving a reduced distance $\geq u$ during a period T is:

$$\Delta Prob(u, T) = \int_0^{D_s} dD_d \int_{u R_E/T}^{\infty} dv N_d(D_d) (\pi u^2 R_E^2 + 2u R_E v T) \frac{v}{v_{rms}^2} e^{-v^2/2v_{rms}^2}. \quad (\text{A2})$$

The integrand is the sum over areas represented in Figure 18. The velocity integral can be done easily, and if the deflectors are effectively confined to a plane, the result can be written as

$$\Delta Prob(u, \xi) = \frac{4G}{c^2} \Sigma D u^2 \left\{ (\pi + 2)e^{-\xi^2/2} + \sqrt{2\pi} \frac{Erfc(\xi/\sqrt{2})}{\xi} \right\}, \quad (A3)$$

where

$$\xi \equiv \frac{uR_E}{v_{rms}T} = u \frac{T_{rms}}{T}, \quad (A4)$$

Σ is the projected surface mass density

$$\Sigma \equiv \int_0^{D_s} m N_d(D_d) dD_d, \quad (A5)$$

and *Erfc* is an error function.

The characteristic crossing time for microlensing is defined by $T_{rms} = R_E/v_{rms} = \sqrt{2r_s D}/v_{rms}$ (see § 3 for definitions) which for Galaxy bulge-bulge lensing is about 10 days (Udalski 2003). For a similar galaxy at redshift $z = 0.05$ lensing a distant SN through its bulge, the reduced distance D is increased by a factor of $\sim 2.7 \times 10^5$ [see § 3.3 and Han & Gould (2003)] and hence T_{rms} increases to $\sim 5,200$ days. If $u \sim 0.05$ and $T = T_{SN} \sim 200$ days, then $\xi \sim 1.3$ and $\Delta Prob(0.05, 1.3) \sim 1.7 \times 10^{-3}$. This particular probability falls off by at least an order of magnitude when $u < 0.01$ or $u > 0.15$.

REFERENCES

- Allen, C. W. 1973, *Astrophysical Quantities* (London: Athone)
- Arnett, D. 1982, *ApJ*, 253, 785
- Arnett, D. 1996, *Supernovae and Nucleosynthesis* (Princeton: Princeton University Press)
- Branch, D., et al. 2005, *PASP*, 117, 545
- Bourassa, R. R., Kantowski, R., & Norton T. D. 1973, *ApJ*, 185, 747
- Bourassa, R. R., & kantowski, R. 1974, *ApJ*, 195, 13
- Bourassa, R. R., & kantowski, R. 1976, *ApJ*, 205, 674
- Chang, K., & Refsdal, S. 1984, *A&A*, 132, 168

- Claret, A., Díaz-Corovés, J., & Giménez, A. 1995, *A&A*, 114, 247
- Cooke, J. H., & Kantowski, R. 1975, *ApJ*, 195, L11
- Han, C., & Gould, A. 2003, *ApJ*, 592, 172
- Höflich, P. 1990, *A&A*, 229, 191
- Jeffery, D. 1999, preprint (astro-ph/9907015)
- Kantowski, R., Vaughan, T., & Branch, D. 1995, *ApJ*, 447, 35
- Kolatt, T. S., & Bartelmann, M. 1998, *MNRAS*, 296, 763
- Linder, E., Schneider, P., & Wagoner, R. V. 1988, *ApJ*, 324, 786
- Mao, S., & Witt, H. J. 1998, *MNRAS*, 300, 1041
- Nomoto, K., Thielemann, F., & Yokoi, K. 1984, *ApJ*, 286, 644
- Oguri, M., Suto, Y., & Turner, E. L. 2003, *ApJ*, 583, 584
- Paczynski, B. 1986a, *ApJ*, 301, 503
- Paczynski, B. 1986b, *ApJ*, 304, 1
- Perlmutter, S., et al. 1999, *ApJ*, 517, 565
- Perlmutter, S., & Schmidt B. P. 2003, *Lecture Notes in Physics*, ed. K. Weiler (Berlin: Springer-Verlag)
- Press, W. H., & Gunn, J. E. 1973, *ApJ*, 185, 397
- Rauch, K. P. 1991, *ApJ*, 374, 83
- Richardson, D., Branch, D., & Baron, E. 2005, *AJ*, submitted
- Riess, A., Press, W. H., & Kirshner, R. P. 1995, *ApJ*, 438, L17
- Schmidt, B. P., et al. 1998, *ApJ*, 507, 46
- Schneider, P., & Wagoner, R. V. 1987, *ApJ*, 314, 154
- Sumi, T., et al. 2003, *ApJ*, 591, 204
- Sumi, T., et al. 2004, *MNRAS*, 348, 1439

Udalski, A. 2003, *Acta Astron.*, 53, 291 (data taken from NOOS & EWS of OGLE III,
<http://www.astrouw.edu.pl/~ogle/>)

Witt, H. J., & Mao, S. 1994, *ApJ*, 430, 505

Wyithe, J. S. B., & Turner, E. L. 2002, *ApJ*, 567, 18

Zakharov, A. F., Popović, L. Č., & Jovanović, P. 2004, *A&A*, 420, 881

Fig. 1.—

Model light curve of a supernova type Ia in its rest frame. Observed data of SN 1990N are added to show the fit.

Fig. 2.—

Microlensing by a point deflector. The deflector’s position is considered as the coordinate origin in the deflector plane.

Fig. 3.—

The position of the primary and secondary images on the deflector plane (angular coordinates) with respect to source and Einstein ring. Note that source makes an angle of 0.04 micro arcsecond with respect to the deflector.

Fig. 4.—

Amplification curves of images of an extended source ($z_s = 1.0$) by a deflector at redshift $z_d = 0.5$. The horizontal axis is the angular separation of deflector and source, β , (see Fig. 3) in micro arcsecond.

Fig. 5.—

Amplification curves of an extended source with a radius of 178 AU, moving at 0.5 AU day^{-1} in the deflector plane. The source reaches its closest approach (impact parameter) at $t = 0$. The figure shows five trajectories with different impact parameters, b (see Fig. 8). For this figure only, the surface brightness and radius are assumed constant.

Fig. 6.—

Normalized IDF profile calculated for SN Ia in U and B bands using W7 model (courtesy of Eric Lentz, University of Georgia), used to calculate the amplification curves of a supernova as an extended source with radius-dependent surface brightness. In this figure, a maximum expansion velocity of $30,000 \text{ km s}^{-1}$ has been used to obtain the expansion velocity projected on the sky. The intensity profile used in the paper is also presented for photospheric speeds of $13,000 \text{ km s}^{-1}$ and $15,000 \text{ km s}^{-1}$.

Fig. 7.—

Expansion speed (*upper panel*) and the radius (*lower panel*) of the photosphere of a type Ia supernova as a function of time.

Fig. 8.—

Geometry of the microlensing model used in § 4.

Fig. 9.—

Alification curve (*upper panel*) and light curve (*lower panel*) of a supernova at $z_s = 1.0$, microlensed by a deflector at $z_d = 0.05$. The input parameters are $m_d = 1 M_\odot$, $v = 0.5 \text{ AU day}^{-1}$, $b = 0.0 r_E$, and $l_o = 0.0 r_E$.

Fig. 10.—

Same as Fig. 9, with input parameters $m_d = 10^{-3} M_\odot$, $v = 0.1 \text{ AU day}^{-1}$, $b = 0.1 r_E$, and $l_o = 0.25 r_E$.

Fig. 11.—

Same as Fig. 9, with input parameters $m_d = 1 M_\odot$, $v = 0.5 \text{ AU day}^{-1}$, $b = 0.01 r_E$, and $l_o = 0.05 r_E$.

Fig. 12.—

Same as Fig. 9, with input parameters $m_d = 10^{-3} M_\odot$, $v = 0.1 \text{ AU day}^{-1}$, $b = 0.1 r_E$, and $l_o = 1.0 r_E$.

Fig. 13.—

Same as Fig. 9, with input parameters $m_d = 10^{-3} M_\odot$, $v = 0.5 \text{ AU day}^{-1}$, $b = 0.01 r_E$, and $l_o = 1.5 r_E$.

Fig. 14.—

Same as Fig. 9, with input parameters $m_d = 10^{-3} M_\odot$, $v = 0.5 \text{ AU day}^{-1}$, $b = 0.1 r_E$, and $l_o = 4.0 r_E$.

Fig. 15.—

Same as Fig. 9, with input parameters $m_d = 1 M_\odot$, $v = 0.5 \text{ AU day}^{-1}$, $b = 0.0 r_E$, and $l_o = 0.1 r_E$.

Fig. 16.—

Same as Fig. 9, with input parameters $m_d = 1 M_\odot$, $v = 0.5 \text{ AU day}^{-1}$, $b = 0.01 r_E$, and $l_o = 0.1 r_E$.

Fig. 17.—

Same as Fig. 9, with input parameters $m_d = 10 M_\odot$, $v = 0.5 \text{ AU day}^{-1}$, $b = 0.0 r_E$, and

$$l_o = 0.05 r_E.$$

Fig. 18.—

Area on the deflector plane within which a microlens would be close enough to a luminous SNe Ia to cause significant changes in its lightcurve.

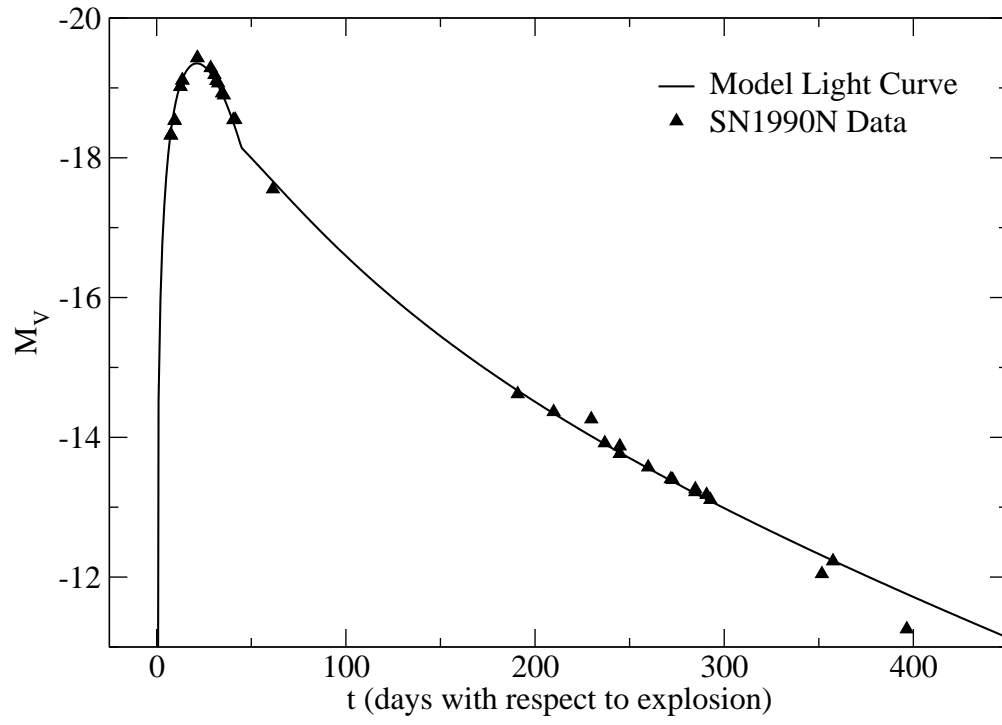


Figure 1

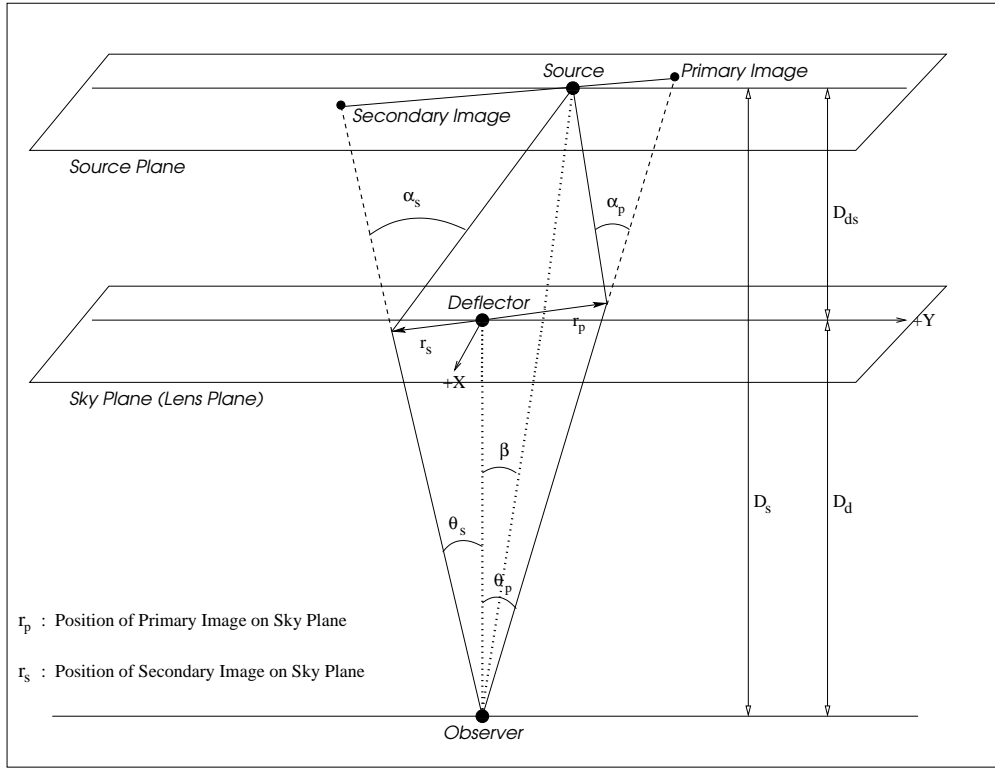


Figure 2

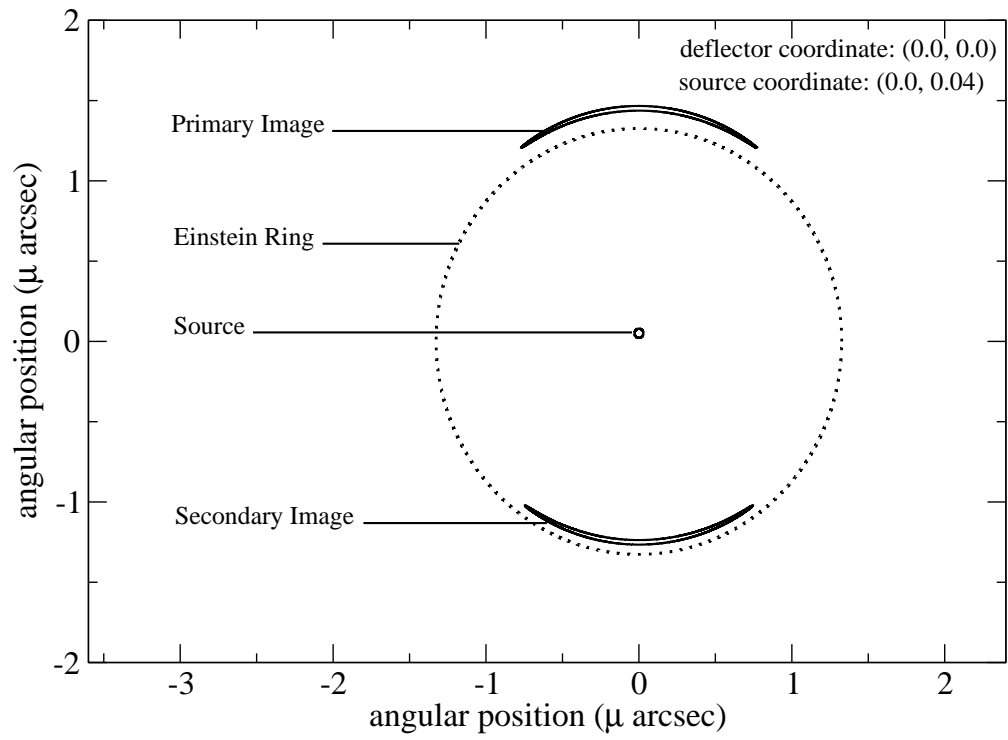


Figure 3

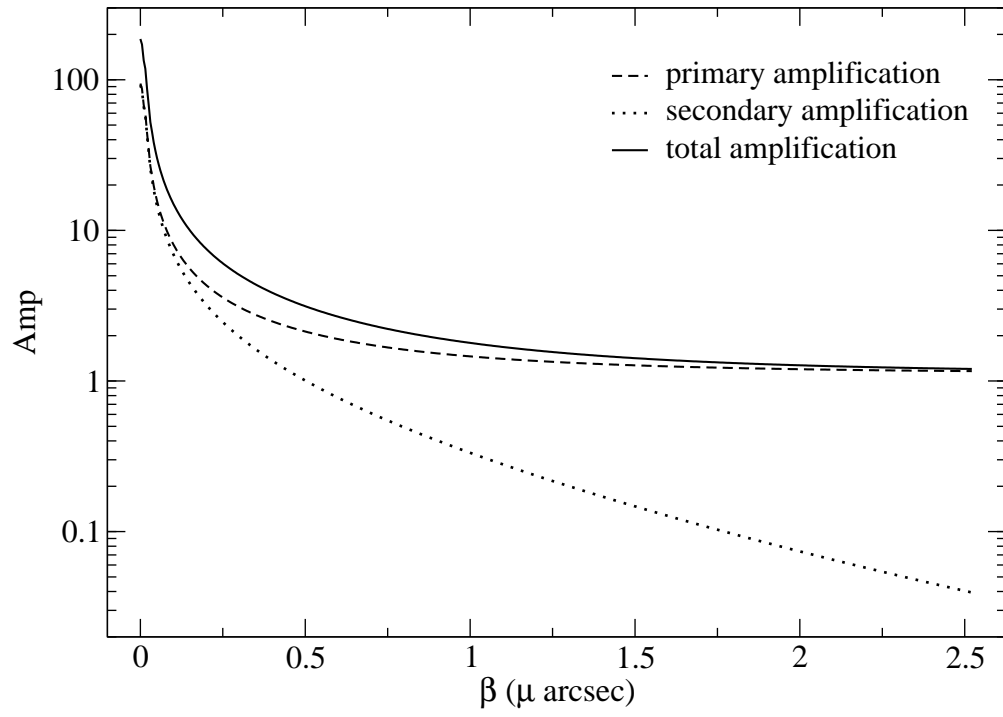


Figure 4

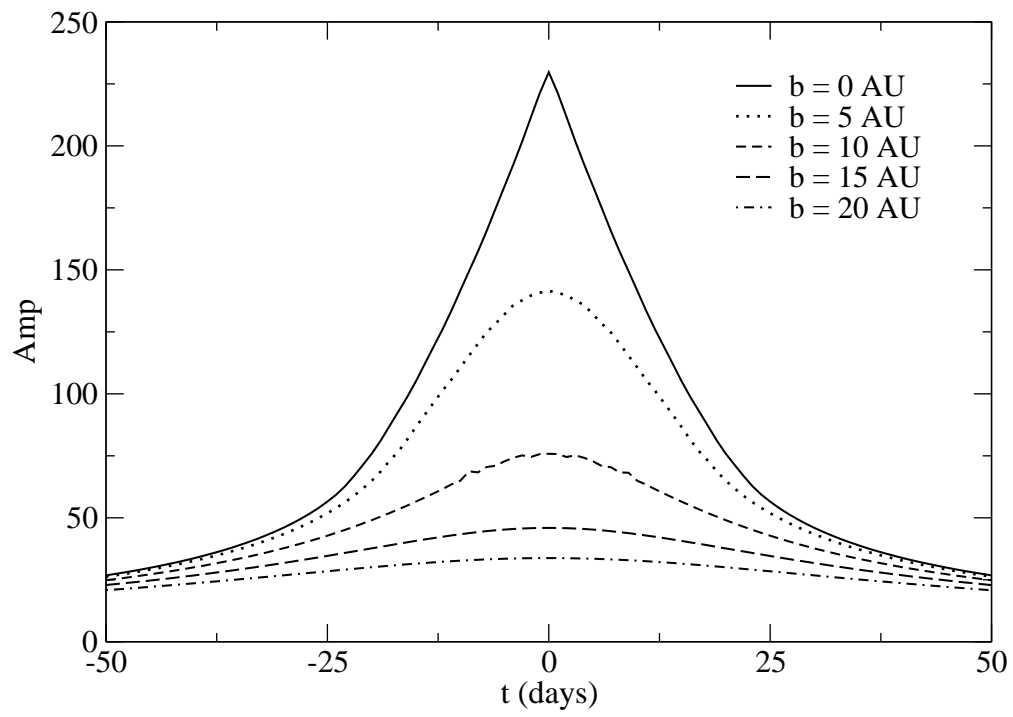


Figure 5

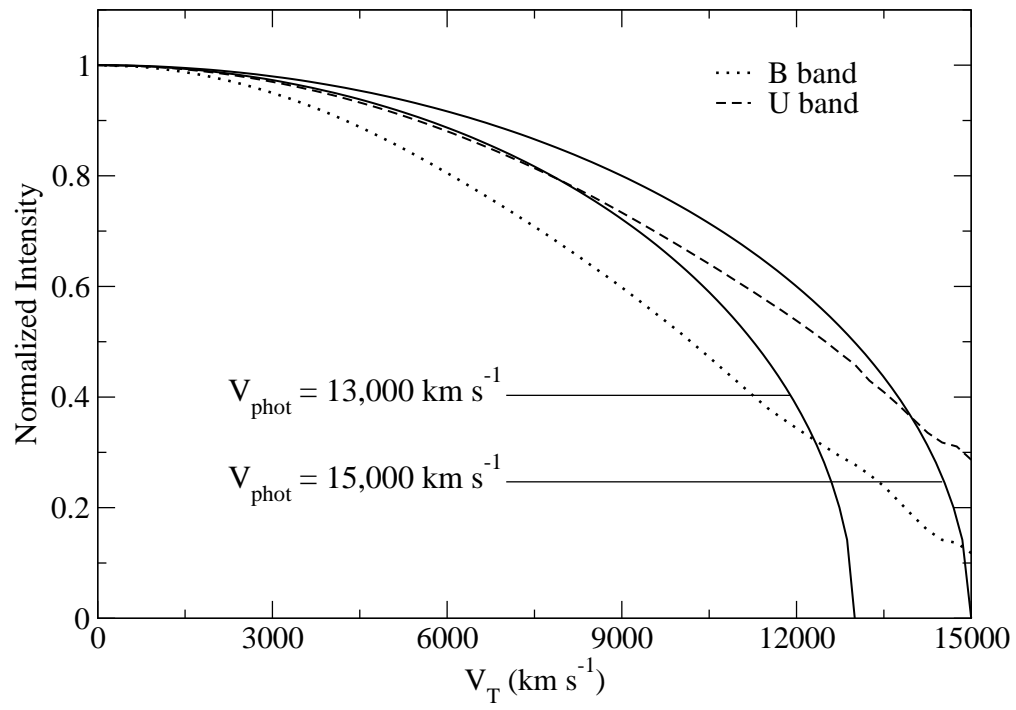


Figure 6

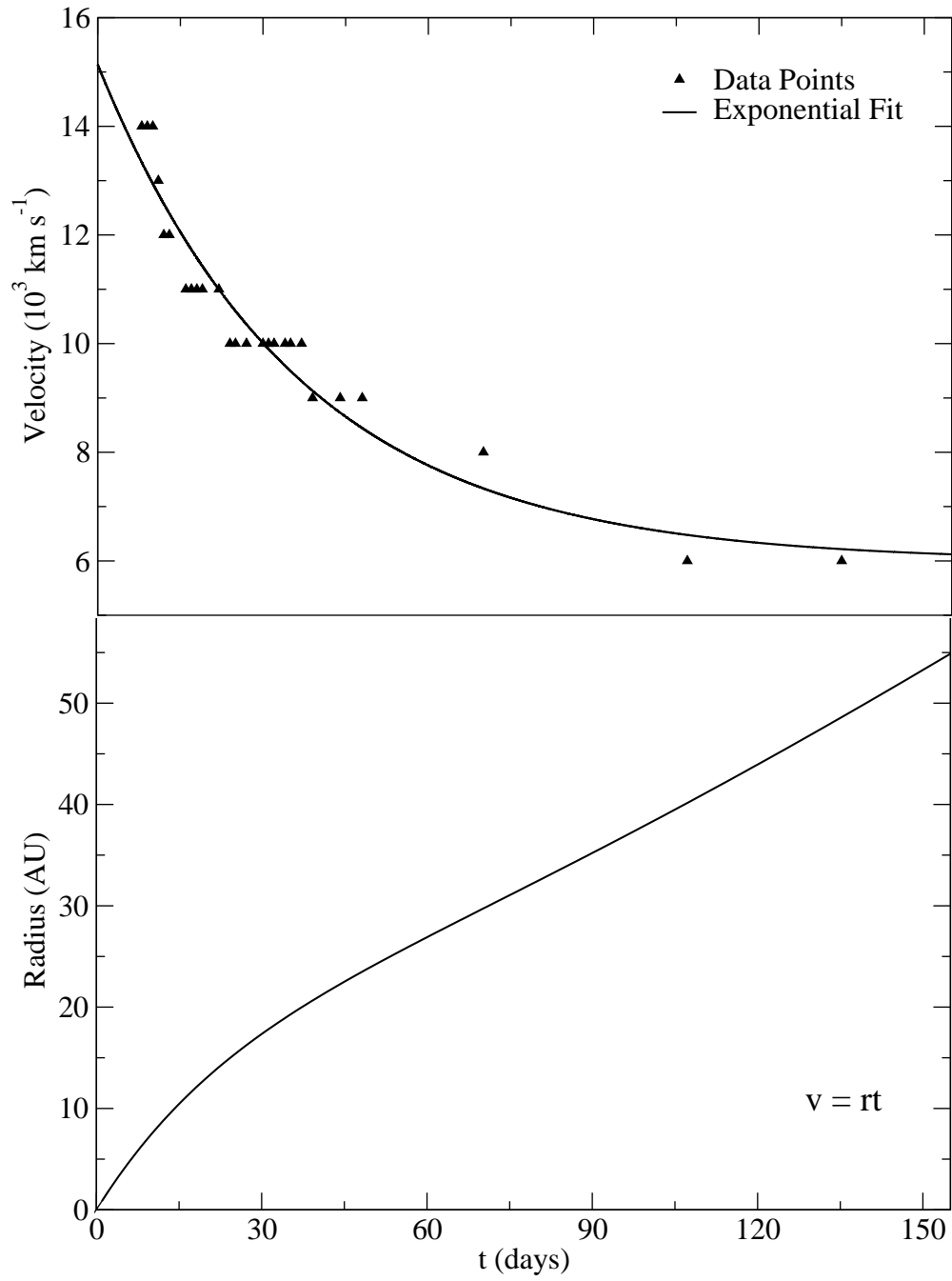


Figure 7

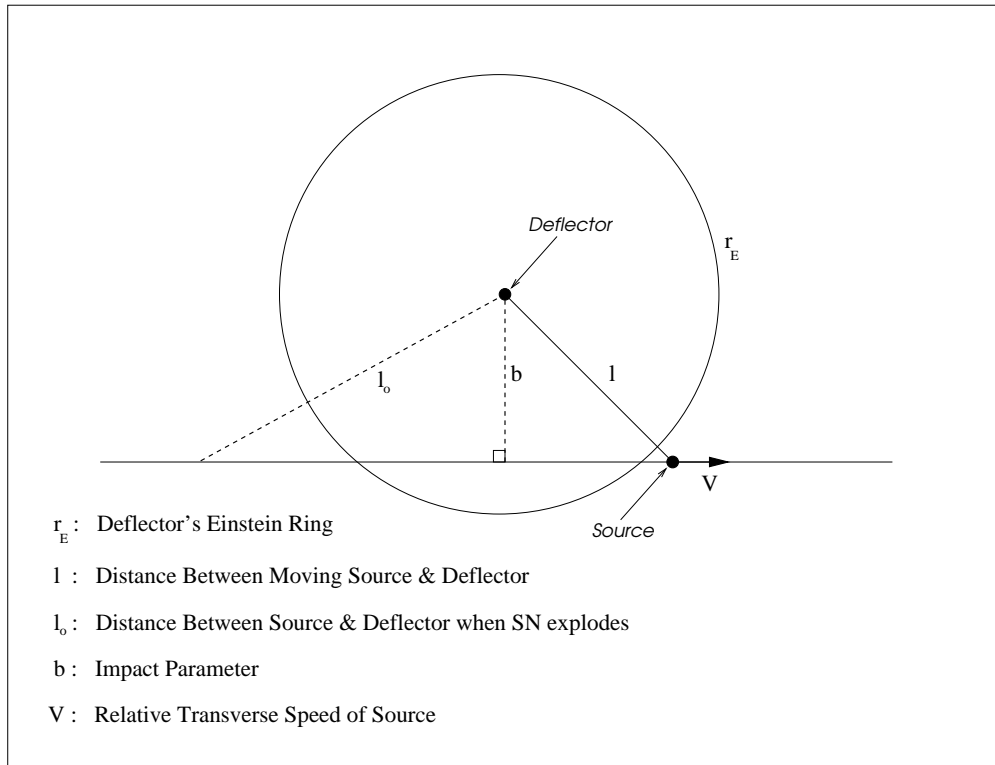


Figure 8

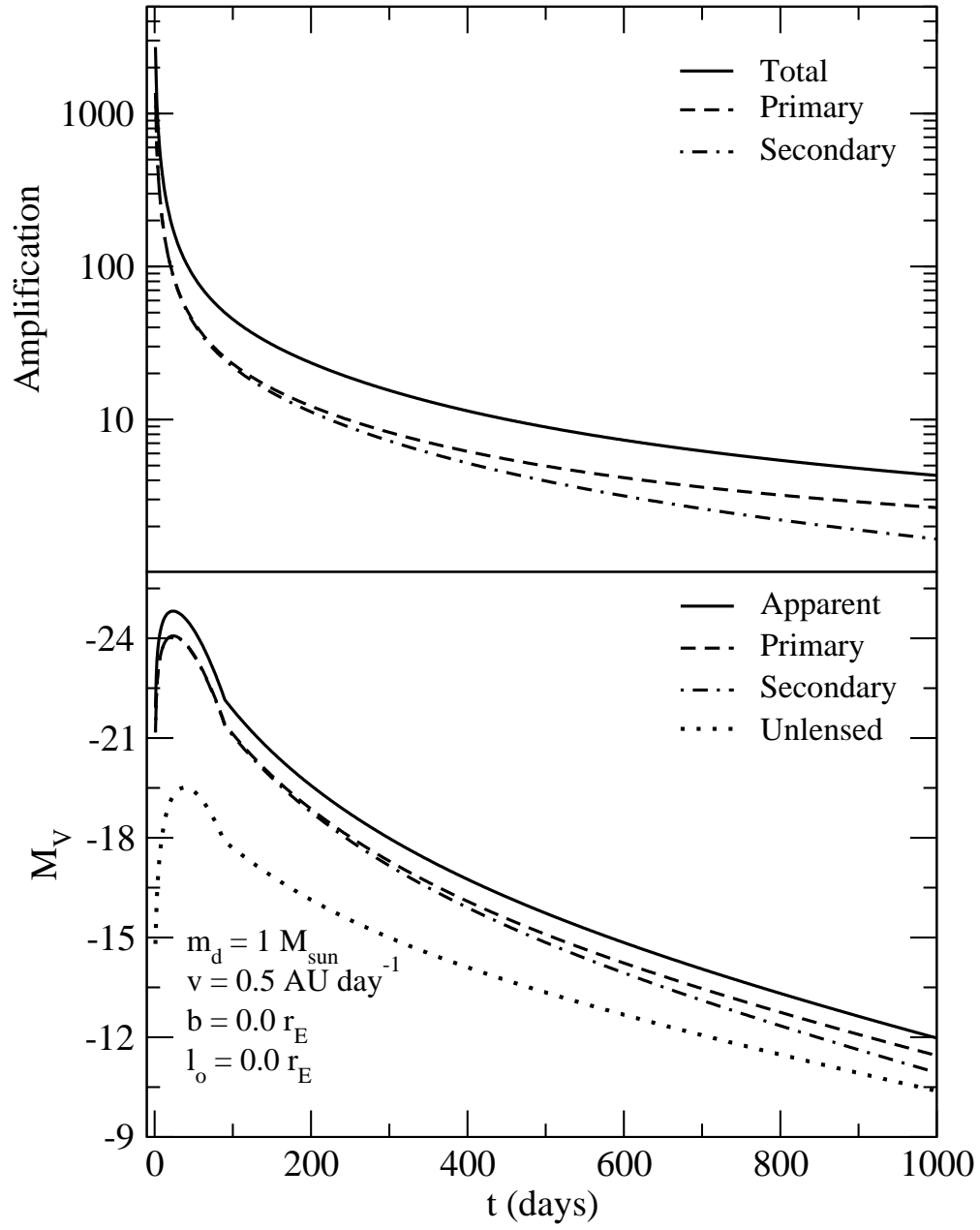


Figure 9

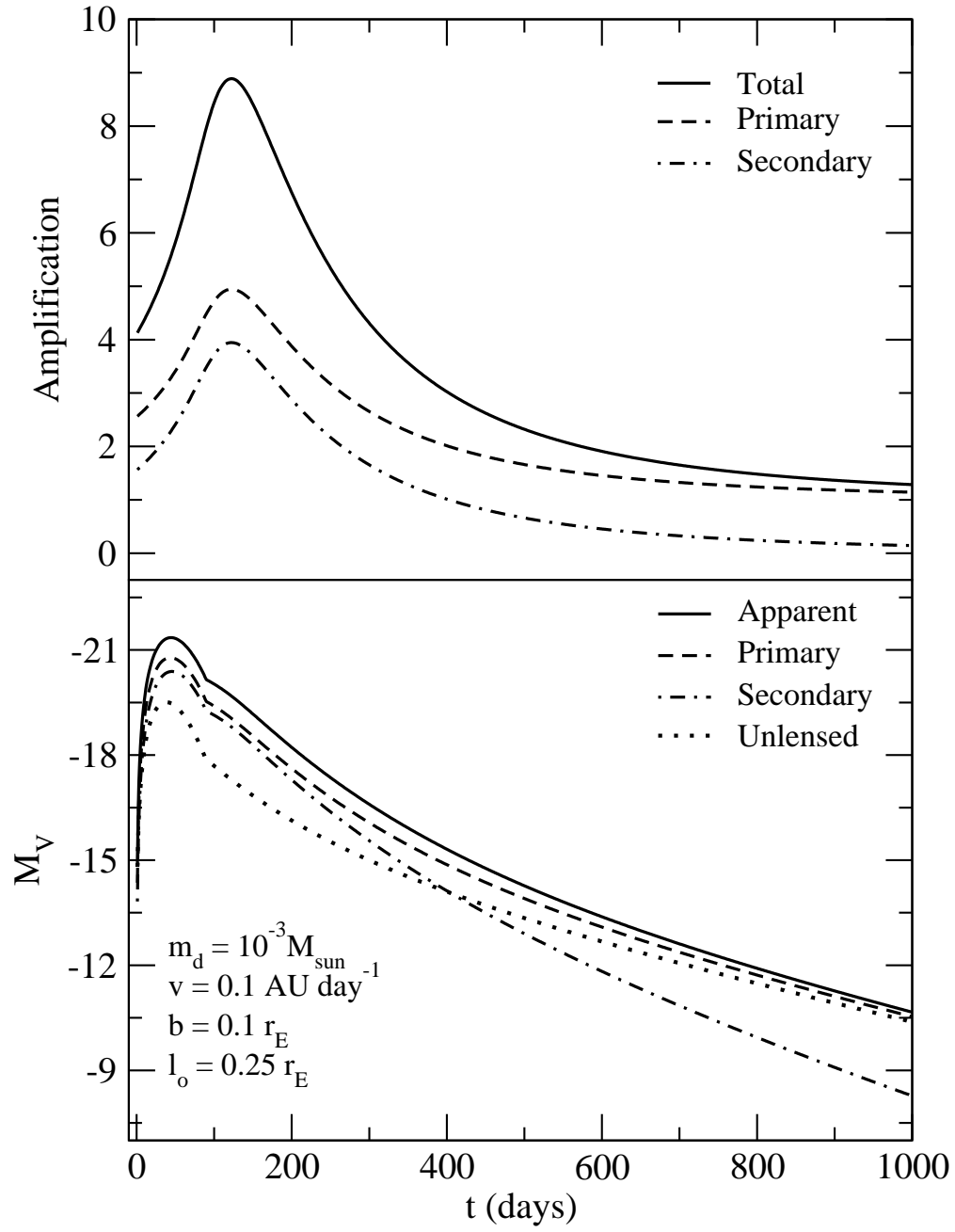


Figure 10

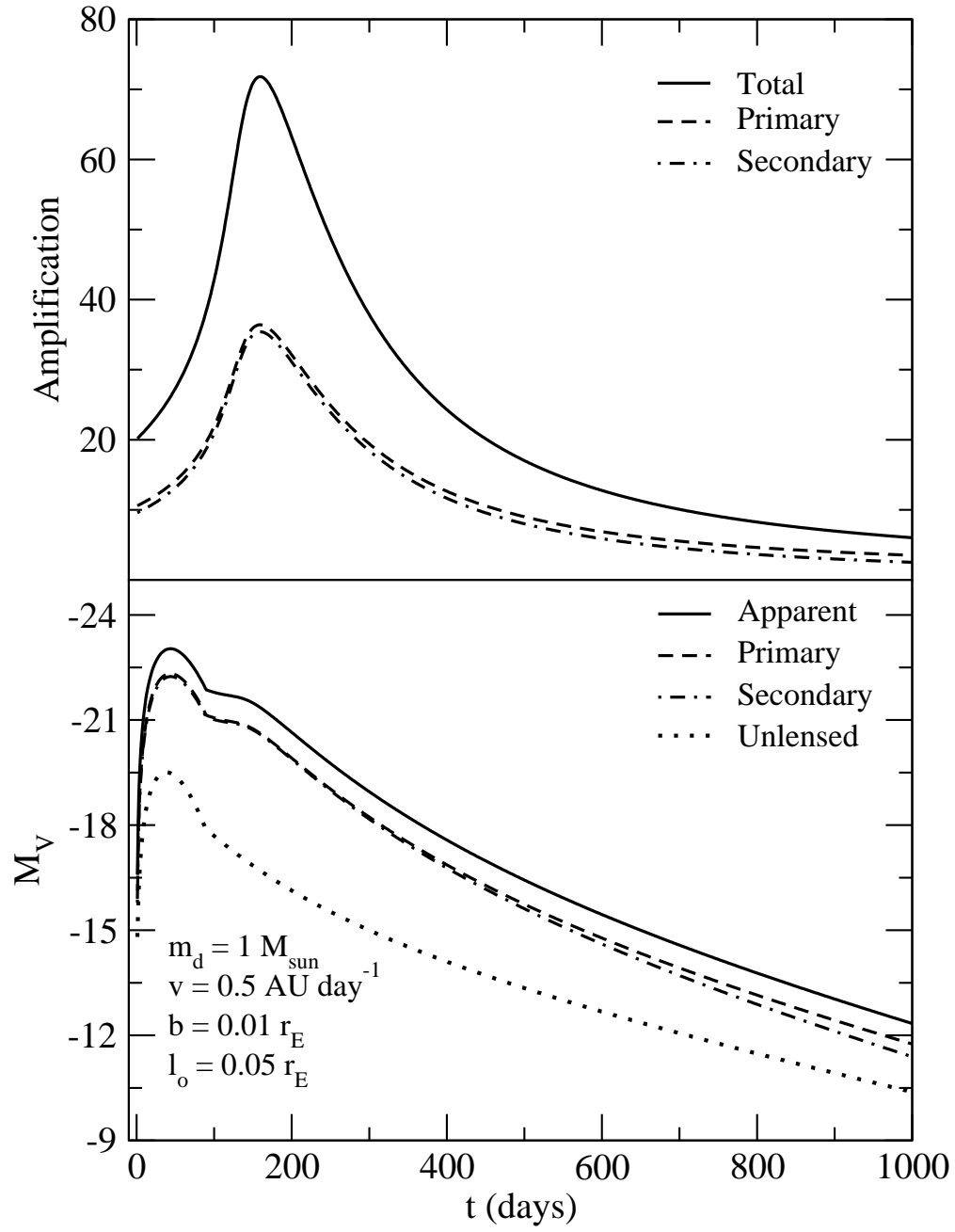


Figure 11

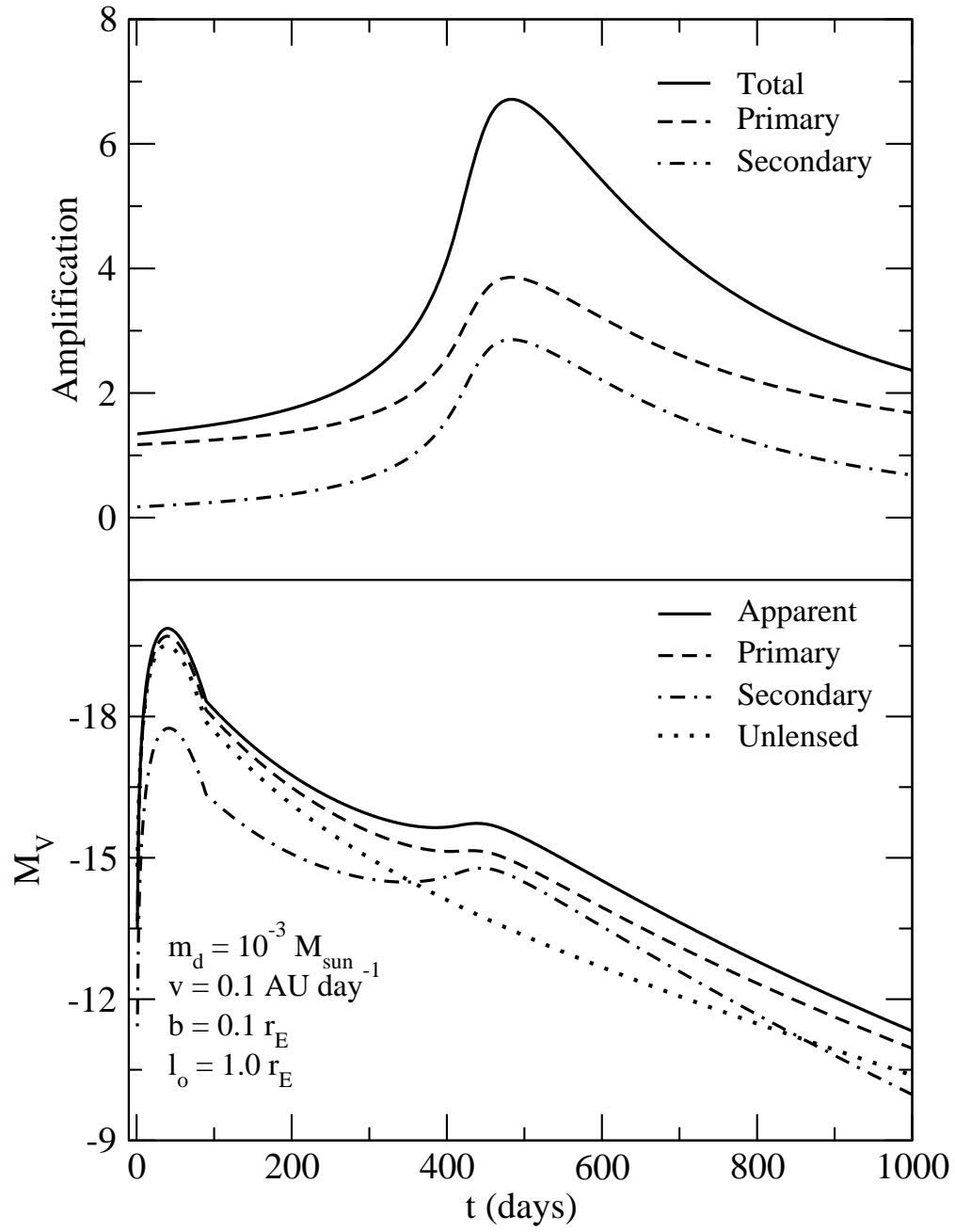


Figure 12

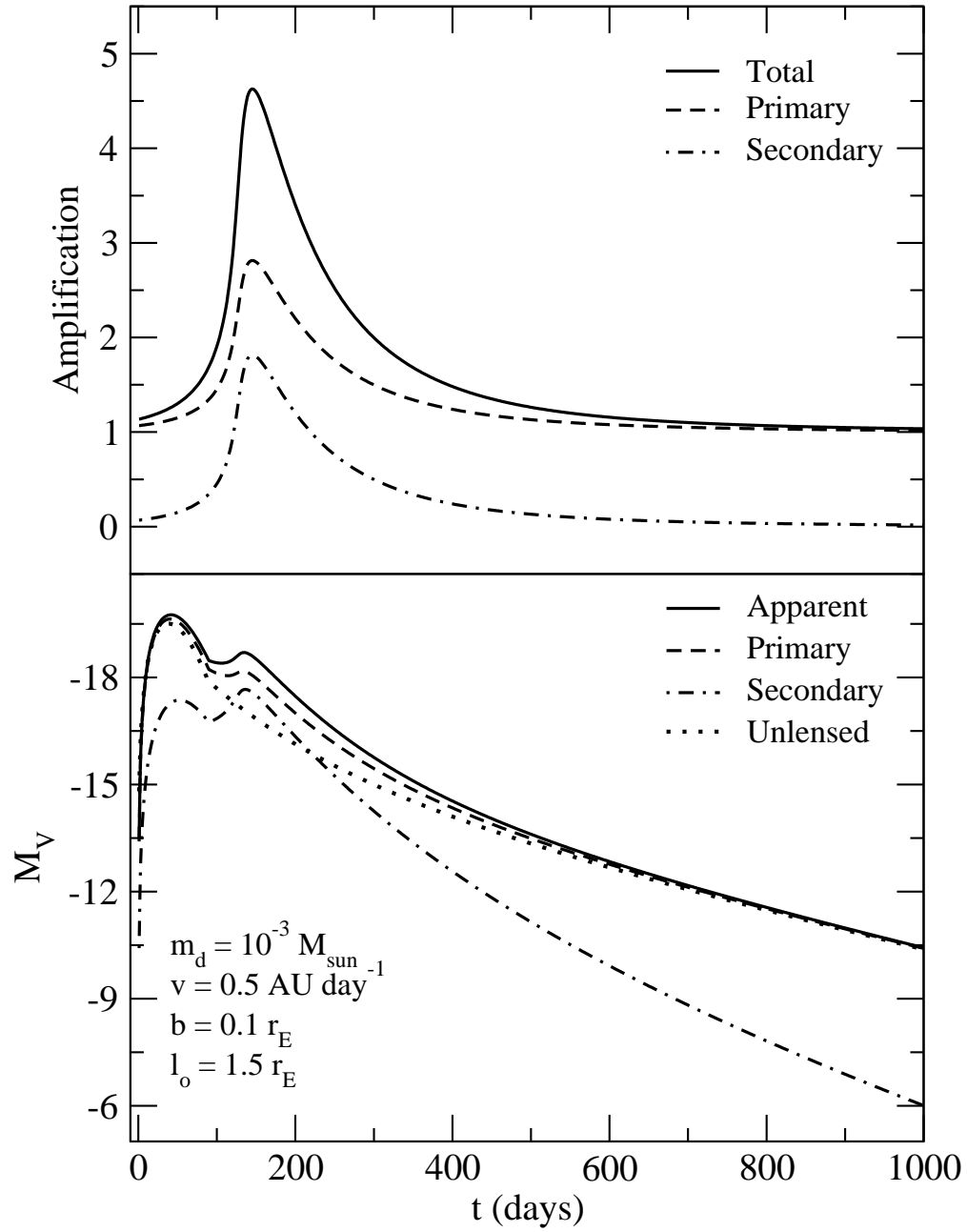


Figure 13

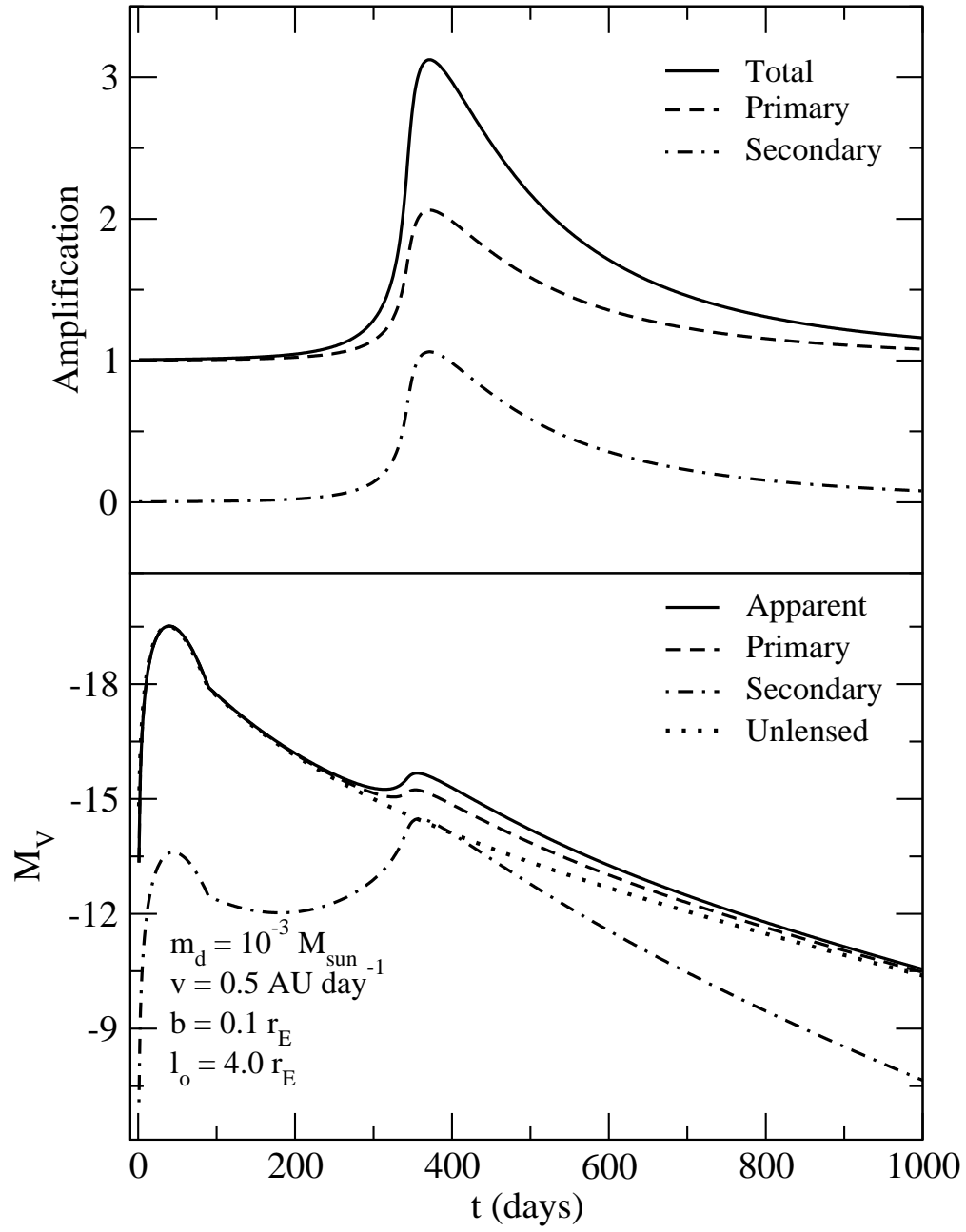


Figure 14

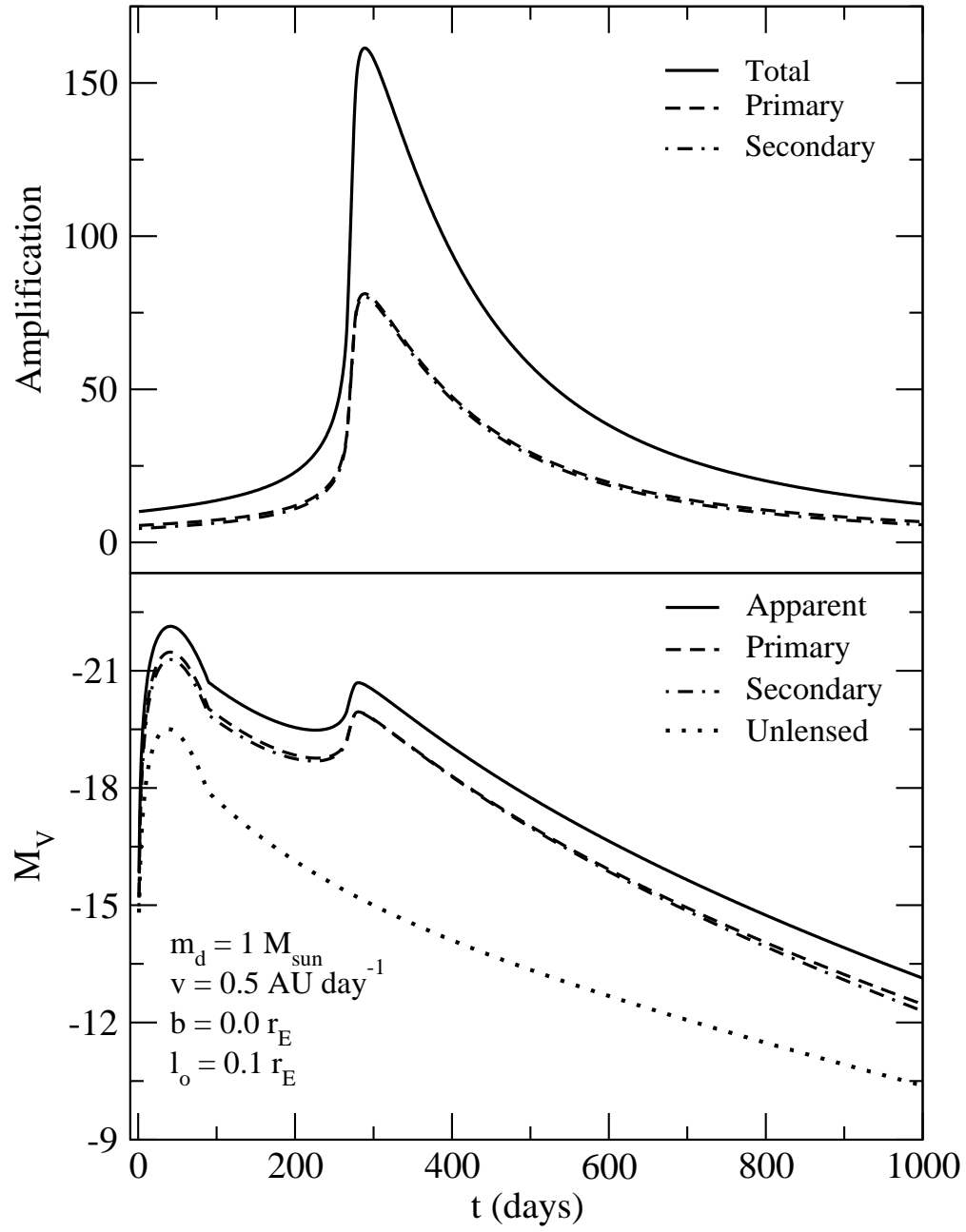


Figure 15

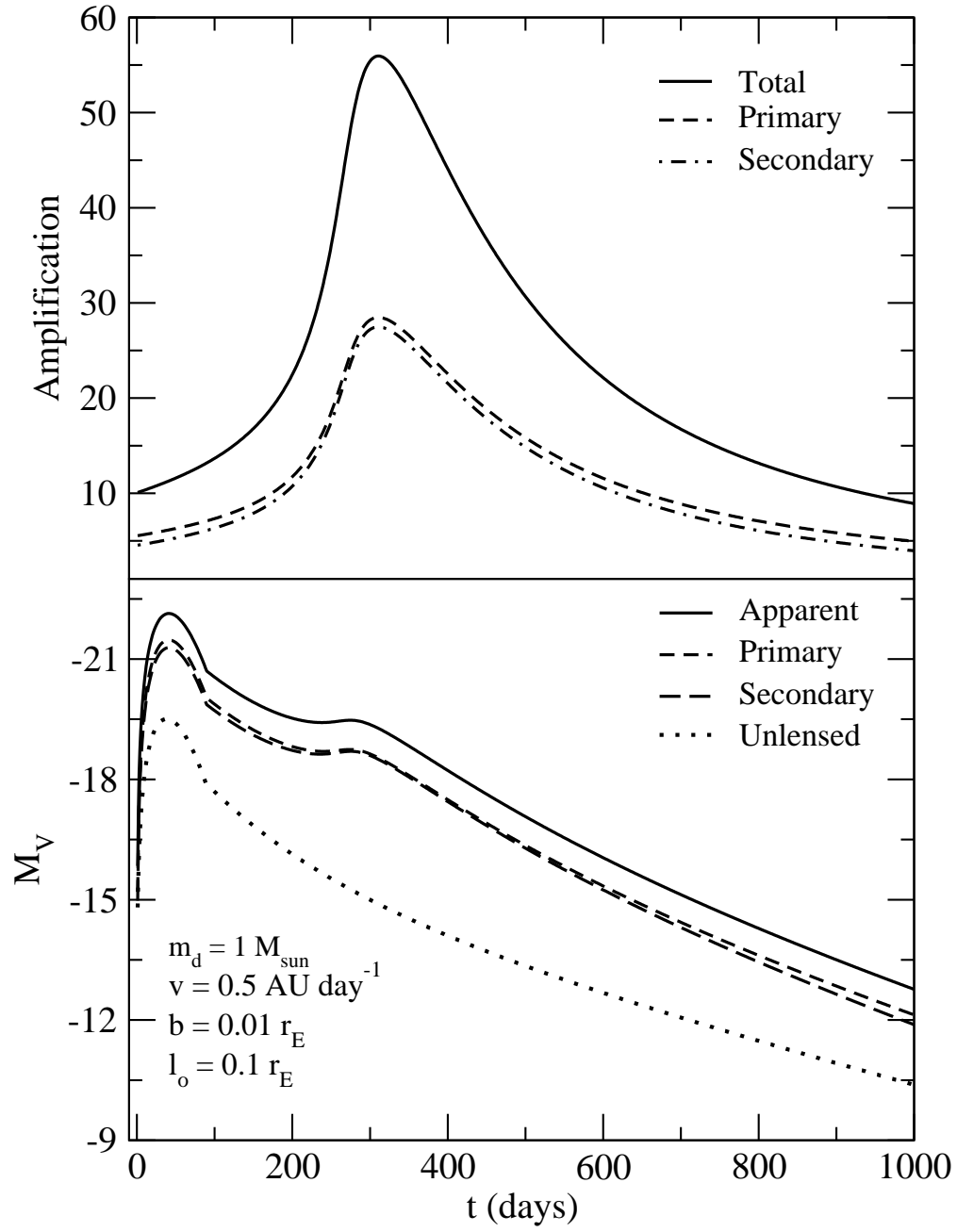


Figure 16

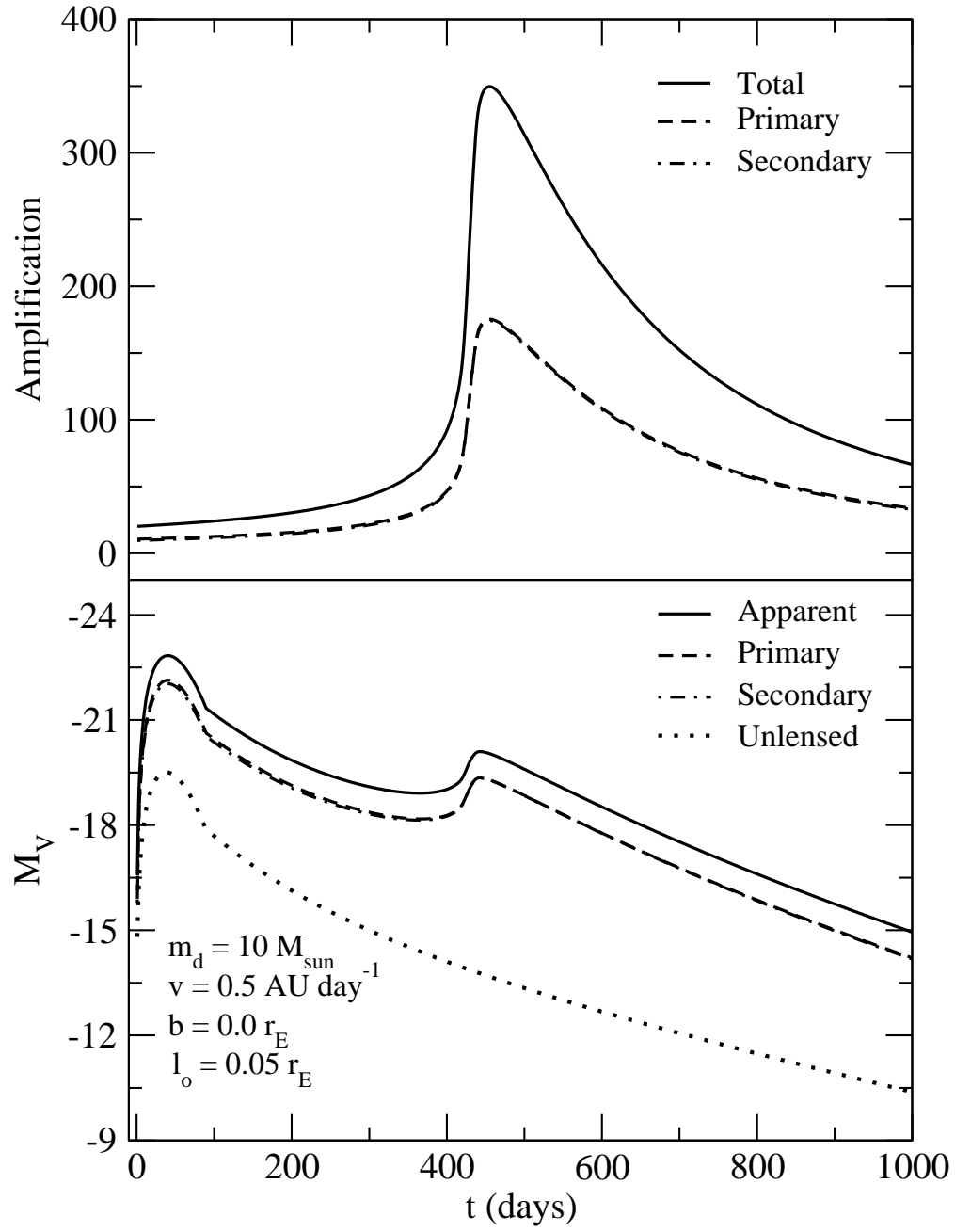


Figure 17

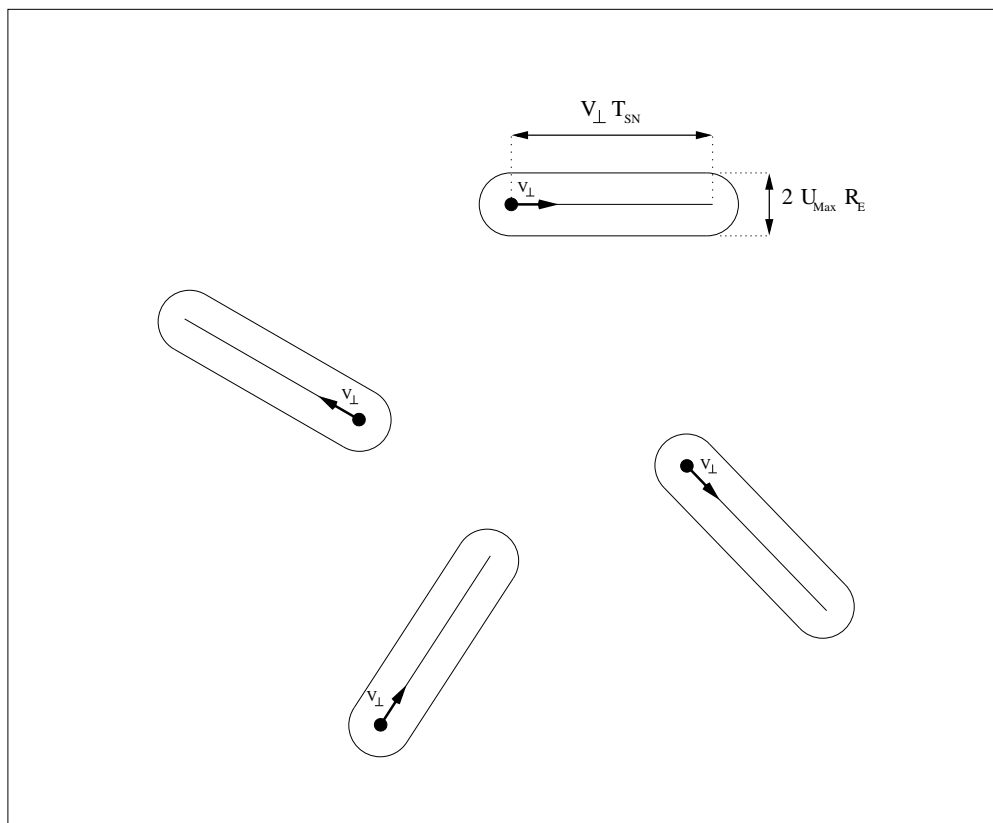


Figure 18